Equivalent-circuit model for slot-effect configuration of an electret-based generator

You may also be interested in:

Equivalent-circuit Models for Electret-based Vibration Energy Harvesters
Cuong Phu Le and Einar Halvorsen

Modeling and characterization of electret based vibration energy harvesters in slot-effect
configuration
M Renaud, G Altena, R Elfrink et al.

Two-Dimensional Simulation of a Dual Frequency Sheath Near an Electrode with a Cylindrical Hole
Dai Zhongling, Liu Chuansheng and Wang Younian

Dynamical Equivalent-Circuit Modeling of MEMS with Squeezed Gas Film Damping
E Westby and T A Fjeldly

Design improvements for an electret-based MEMS vibrational electrostatic energy harvester
G Altena, M Renaud, R Elfrink et al.

Analysis and design of the taper in metal-grating periodic slow-wave structures for rectangular
Cerenkov masers
Chen Ye, Zhao Ding, Wang Yong et al.

Improvement on the wave absorbing property of a lossy frequency selective surface absorber using a
magnetic substrate
Sun Liang-Kui, Cheng Hai-Feng, Zhou Yong-Jiang et al.

Performance Analysis and Development Strategies for Solid Oxide Fuel Cells
E Ivers-Tiffée, A Leonide and A Weber

Equivalent-circuit model for slot-effect configuration of an electret-based generator

Cuong Phu Le[1], Michael Renaud[2] and Einar Halvorsen[1]

[1]Univ. College of Southeast Norway, Norway, [2]IMEC/Holst Centre, The Netherlands

E-mail: `Einar.Halvorsen@hbv.no`

Abstract. This paper presents a completely analytical method to build a lumped-model for an electret-based energy harvester. The harvester consists of two patterned electrodes facing movable electret patterns in a slot-effect electrical scheme. A Chebyshev expansion with orthogonal functions to capture singularity effects and Galerkin's method are used to determine fundamental parameters of the equivalent circuit. All important fringing fields in the microscale device are thereby taken into account. For a device example, the calculated parameters of the model agree well with those obtained by finite element modelling. The dynamic behaviour is reproduced by the established model. The advantage of the approach is to allow a fast and full exploration of the design parameters for optimization of the device structure.

1. Introduction

Biasing of electrostatic vibration energy harvesters is an essential feature for their operation. For a full MEMS integration, internal bias by an electret, which is a dielectric with trapped charges [1], is favourable over external bias by circuitry. A number of recent investigations on MEMS electret-based vibration energy harvesters consider devices configured as a set of metal-strip electrodes and a patterned electret on two separate substrates [2, 3, 4, 5]. Such a device concept has potential applications in car-tire pressure monitoring [6, 7, 8].

Modelling of electret-based harvesters is challenging when electrostatic fringing field effects are significant. Several groups have developed models and guidelines for device optimization. These models can be made either by using an ideal field approximation, which is inaccurate, or by time-consuming finite element computations [9, 10, 11]. Conformal mapping techniques can be a solution, but are limited by assumption on geometry and material [12]. An improved model by [13] included closed-form parasitic capacitances using an effective permittivity to represent the dielectric media surrounding the electrodes. The effect of the electret substrate was ignored even when the gap between the two substrates was small.

In the present work, the aforementioned limitations are overcome by developing an accurate and fully analytic method to build an equivalent lumped-model for the harvester. The method used here is adapted from our previous work [14] that includes electrostatic nonlinearities and fringing fields. The harvester parameters reported in [15] are used for example calculations that illustrate the method.
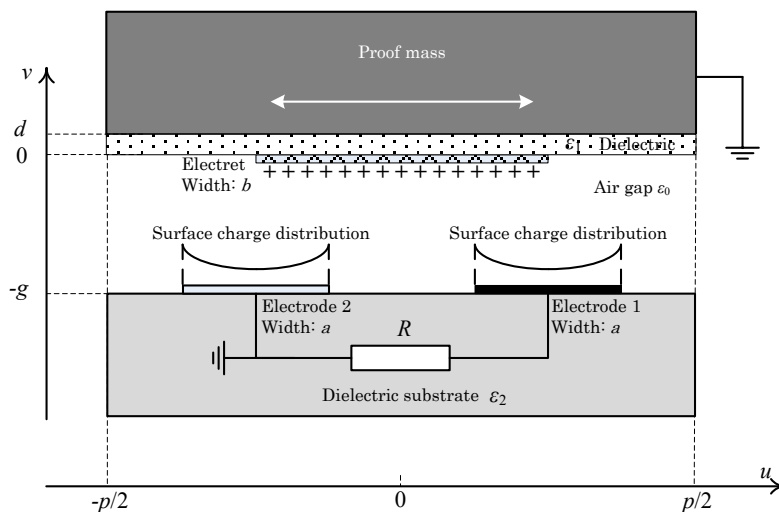
Figure 1. Cross-section of a single period for an electret-based vibration energy harvester.

2. Transducer description

Figure 1 shows a simplified cross-section of one period p for the electret-based transducer. The transducer consists of N pairs of metal electrodes 1 & 2 on a dielectric substrate with a permittivity ε_2 that face electret patterns deposited on a dielectric layer with a permittivity ε_1 and a thickness d. The dielectric layer ε_1 is supported by a conductive substrate functioning as a proof mass m suspended by mechanical springs (not shown) with a total stiffness k. The medium gap g between two substrates has a permittivity ε_0. The metal electrode and electret patterns have a width of a and b respectively. Each pattern has a length L. The electret has a total fixed charge $Q_{\mathrm{e}} = \frac{\varepsilon_1 b N L}{d} V_{\mathrm{e}}$, where V_{e} is an equivalent average surface voltage over the electret patterns.

There are several schemes for power extraction based on the arrangement of connections between the three electrical terminals, i.e the two electrodes and the conductive proof mass. A typical configuration is the slot-effect scheme [12, 15, 16] where a load, e.g. a resistor R, is connected between the two electrodes 1 & 2 and one of them is grounded together with the conductive proof mass as shown in figure 1. When the proof mass oscillates in the lateral direction, the charged electret induces varying charges on the counter electrodes and then generates an electrical current through the resistor R.

3. Analysis and modelling

In the analysis, we assume that all electrode and electret patterns are sufficiently thin that they can be treated as zero thickness. The number N of periods is large enough that end-effects can be ignored. To capture fringing fields, the surface charges induced on the electrodes are mathematically represented by an orthogonal expansion in Chebyshev polynomials multiplied by a reciprocal square root form, i.e.

$$
\sigma_{1,2}(u) = \begin{cases} \sum_{n=0}^{N} C_n^{1,2} \phi_n^{1,2}(u) = \sum_{n=0}^{N} C_n^{1,2} \dfrac{T_n\left(\frac{2\left(u \mp \frac{p}{4}\right)}{a}\right)}{\sqrt{1 - 4\frac{(u \mp \frac{p}{4})^2}{a^2}}} & -\frac{a}{2} \leq u \mp \frac{p}{4} \leq \frac{a}{2} \\ 0 & \text{elsewhere} \end{cases} \tag{1}
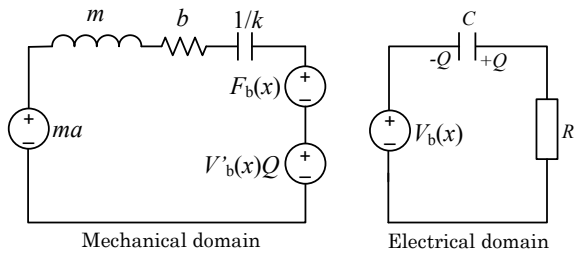$$

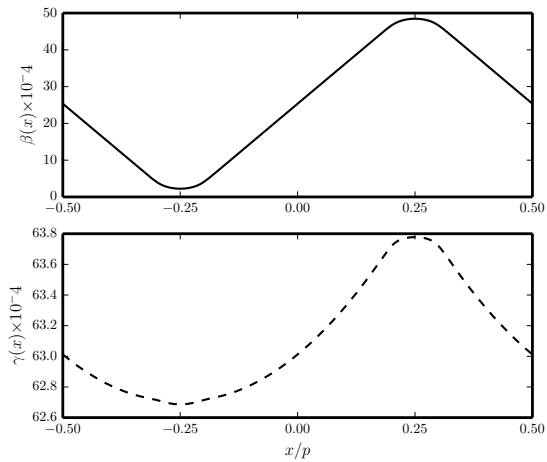**Figure 2.** Lumped-model of electret-based transducer.

Figure 3. Induced-charge coefficients as function of proof mass displacement.

where N is a maximum Chebyshev index, $T_n(u)$ are Chebyshev polynominals of degree n=0, 1, ..., N, $\{C_n^1\}$ and $\{C_n^2\}$ are expansion coefficients. The total charges on electrodes 1 & 2 are

$$Q_{1,2} = NL \int_{-p/2}^{p/2} \sigma_{1,2}(u)du = NL\frac{\pi a}{2}C_0^{1,2}. \tag{2}$$

From here, the analytical approach to establish parameters for the equivalent circuit model can be briefly described as follows. First, Laplace's equation $\nabla^2\varphi(u,v) = 0$ is used to find the potential distributions on two substrate surfaces $\varphi(u,0)$ and $\varphi(u,-g)$. The Galerkin method with the reciprocal root form as a weight function in Eq. (1) is then employed to enforce constant potential boundary on two electrodes $V_1 = V_R$ and $V_2 = 0$ V. Now, the expansion coefficients $\{C_n^1\}$ and $\{C_n^2\}$ can be found by solving the resulting set of equations. Further details on procedure to determine the expansion coefficients can be found in [14]. As a result, the total electrostatic energy is

$$W_e(x,Q) = \frac{1}{2}\begin{bmatrix} Q_1 & Q_2 \end{bmatrix}\begin{bmatrix} V_1 \\ V_2 \end{bmatrix} + \frac{1}{2}NL\int_{-\frac{p}{2}+x}^{\frac{p}{2}+x}\varphi(u,0)\sigma_e(u)du \tag{3}$$

where the last term in the above equation is the electret energy with $\sigma_e(u) = \frac{Q_e}{bNL}$ for $-b/2 \le u - x \le b/2$. With the charge $Q = Q_1$ as the generalized displacement in the electrical domain, the energy W_e can be written on the form

$$W_e(x,Q) = \frac{\alpha}{4\pi\varepsilon_0 NL}Q^2 + \frac{\beta(x)}{2\pi\varepsilon_0 NL}QQ_e + \frac{\gamma(x)}{4\pi\varepsilon_0 NL}Q_e^2 \tag{4}$$

where the coefficients α, $\beta(x)$, and $\gamma(x)$ are dimensionless and dependent on the geometry, the transducer materials and the proof mass displacement. The corresponding electrostatic force acting on the proof mass and the voltage across the resistance R are

$$F_e = \frac{\partial W_e(x,Q)}{\partial x} = \frac{\beta'(x)}{2\pi\varepsilon_0 NL}QQ_e + \frac{\gamma'(x)}{4\pi\varepsilon_0 NL}Q_e^2 = V_b'Q + F_b(x) \tag{5}$$
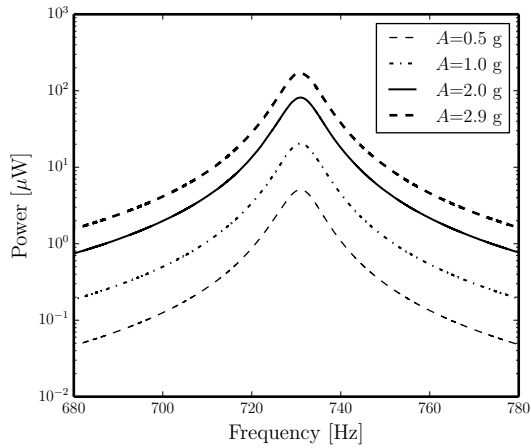
Figure 4. Frequency responses of output power for various acceleration amplitudes at $V_{\mathrm{e}} = 160$ V and $R = 5.0$ MΩ.
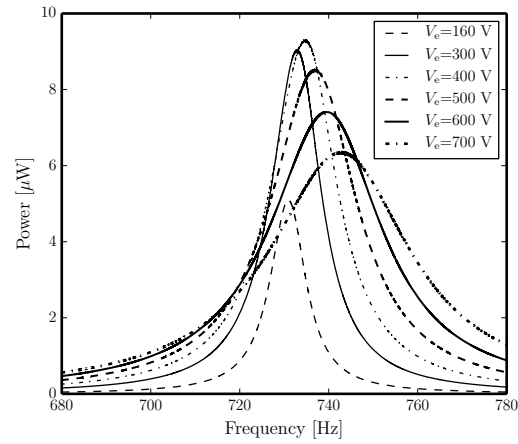

Figure 5. Effect of electret voltage V_{e} on frequency response at $A = 0.5$g and $R = 5.0$ MΩ.
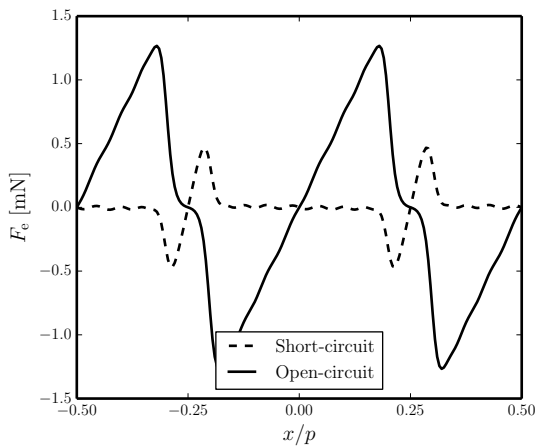

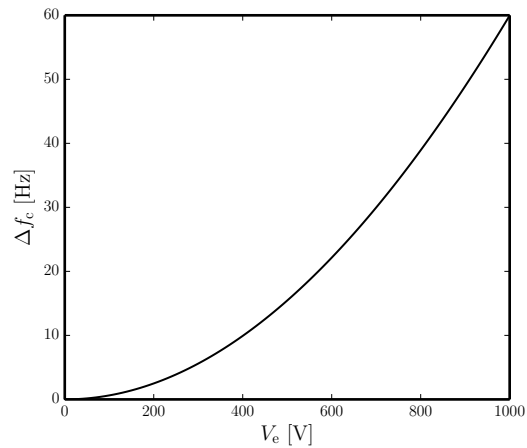**Figure 6.** Electrostatic force for short-circuit and open-circuit conditions at $V_{\mathrm{e}} = 160$ V.

Figure 7. Center frequency shift at open circuit when increasing electret voltage V_{e}.

and

$$V_{\mathrm{R}} = \frac{\partial W_{\mathrm{e}}(x, Q)}{\partial Q} = \frac{\alpha}{2\pi\varepsilon_0 NL}Q + \frac{\beta(x)}{2\pi\varepsilon_0 NL}Q_{\mathrm{e}} = \frac{1}{C}Q + V_{\mathrm{b}}(x) \tag{6}$$

where $C = \frac{2\pi\varepsilon_0 NL}{\alpha}$, $F_{\mathrm{b}}(x) = \frac{\gamma'(x)}{4\pi\varepsilon_0 NL}Q_{\mathrm{e}}^2$ and $V_{\mathrm{b}}(x) = \frac{\beta(x)}{2\pi\varepsilon_0 NL}Q_{\mathrm{e}}$.

By including the inertial force $F_{\mathrm{ext}} = ma$ and mechanical damping b, the dynamics of the harvester can be represented by the equivalent circuit as shown in figure 2.

4. Device example and simulation results

We use the parameters of the device in [15] as an example. The calculation gives $\alpha = 0.2147$ and displacement-dependent functions $\beta(x)$ and $\gamma(x)$ as shown in figure 3. It can be seen that the transducer has the maximum and minimum stored energy when the proof mass displacement are at two extremes $\pm\frac{p}{4}$. The found parameters result in $C = 51.8$ pF and $Q_0 = -3.26$ nC while the

corresponding values obtained by finite elemement computation in [15] were $C^{\text{FEM}} = 52.5$ pF and $Q_0^{\text{FEM}} = -3.2$ nC, where Q_0 is the equilibrium charge of Q. This agreement validates the calculation approach that takes all effects of the fringing fields into account.

Figure 4 shows frequency responses of the harvester for different acceleration amplitudes at $V_e = 160$ V and $R = 5.0$ MΩ. The behaviour reproduced by the model is in agreement with experimental results, but the power obtained from the simulation is smaller by about 15% than the measured power in [15]. Apart from the accuracy of the experimental model parameters, the deviation can be explained by the measured device having a corrugated electret while the analysis is based on a patterned flat electret.

The effect of the surface voltage V_e on the output power is shown in figure 5. An optimal voltage around $V_e = 400$ V is found when increasing from 160 V while holding the acceleration amplitude fixed. Further increase of V_e reduces the power due to the stronger electrostatic force that limits the proof mass displacement. In addition, the electrostatic nonlinearity caused by increasing V_e shifts center-frequency upwards. This can be explained by analysis of the electrostatic force at short- and open-circuit conditions as shown in figure 6. There is almost no stiffness contribution from the electrostatic force at shorted circuit. With open circuit, the system stiffness is higher because of the additional force $F_e^{\text{open}} \approx 14.1$ N/m $\times x$ around the equilibrium position. Thus, the nonlinearity moves the center frequency by Δf_c as shown in figure 7 and can be used to adapt the harvester to the ambient vibration frequency.

5. Conclusion

A fully analytical method that provides induced-charge coefficients for electret-based energy harvesters in the slot-effect configuration was presented. From this method, an equivalent circuit model that takes into account effects of fringing fields and electrostatic transducer nonlinearities followed. The key model parameters can be simply calculated from the induced-charge coefficients. Variations on the proposed approach for other configurations of electret-based harvesters and further optimization on transducer geometry are left for future work.

References

[1] Suzuki Y 2011 *IEEJ Trans. Elec. Electron Eng.* **6** 101--111
[2] Sakane Y, Suzuki Y and Kasagi N 2008 *J. Micromech. Microeng.* **18** 104011
[3] Edamoto M, Suzuki Y et al. 2009 *Proc. IEEE MEMS2009 (Sorrento, January)*, 1059–1062
[4] Narsure Y, Matsubara N et al. 2009 *J. Micromech. Microeng.* **19** 094002
[5] Chiu Y and Lee Y C 2013 *J. Micromech. Microeng.* **23** 015012
[6] Westby E R and Halvorsen E 2012 *IEEE/ASME Trans. Mechatronics* **17** 995–1005
[7] Renaud M, Altena G et al. 2013 *Proc. Transducer2013, (Barcelona, June)*, 693–696
[8] Elfrink R, Van Acht V et al. 2014 *Proc. SSI2014* 69-76
[9] Boland J, Chao Y H et al. 2003 *Proc. IEEE MEMS2003 (Kyoto, January)*, 538–541
[10] Bartsch U, Sander C et al. 2009 *Proc. PowerMEMS2009 (Washington DC, December)* 332–335
[11] Boisseau S, Despesse G and Sylvestre A 2010 *Smart Mater. Struct.* **19** 075015
[12] Okamoto H, Hamate Y and Kuwano H 2012 *Smart Mater. Struct.* **21** 065001
[13] Chen R and Suzuki Y 2013 *J. Micromech. Microeng.* **23** 125015
[14] Le C P and Halvorsen E 2013 *J. Intell. Mater. Syst. Struct.* **24** 1176–1186
[15] Renaud M, Altena G et al. 2015 *Smart Mater. Struct.* **24** 085023
[16] Perez M, Boisseau S et al. 2016 *Smart Mater. Struct.* **25** 045015